



HAL
open science

Apical and basal auxin sources pattern shoot branching in a moss

Mattias Thelander, Katarina Landberg, Arthur Muller, Gladys Cloarec, Nik
Cunniffe, Stéphanie Huguet, Ludivine Soubigou-Taconnat, Véronique
Brunaud, Yoan Coudert

► **To cite this version:**

Mattias Thelander, Katarina Landberg, Arthur Muller, Gladys Cloarec, Nik Cunniffe, et al.. Apical and basal auxin sources pattern shoot branching in a moss. 2022. hal-03515264

HAL Id: hal-03515264

<https://hal.science/hal-03515264v1>

Preprint submitted on 6 Jan 2022

HAL is a multi-disciplinary open access archive for the deposit and dissemination of scientific research documents, whether they are published or not. The documents may come from teaching and research institutions in France or abroad, or from public or private research centers.

L'archive ouverte pluridisciplinaire **HAL**, est destinée au dépôt et à la diffusion de documents scientifiques de niveau recherche, publiés ou non, émanant des établissements d'enseignement et de recherche français ou étrangers, des laboratoires publics ou privés.

1 **Apical and basal auxin sources pattern shoot branching in a moss**

2

3

4 Mattias Thelander¹, Katarina Landberg¹, Arthur Muller^{2,3}, Gladys Cloarec^{2,4}, Nik Cunniffe⁵,
5 Stéphanie Huguet^{6,7}, Ludivine Soubigou-Taconnat^{6,7}, Véronique Brunaud^{6,7} and Yoan
6 Coudert^{2,*}

7

8 ¹Department of Plant Biology, Swedish University of Agricultural Sciences, The Linnean Centre for
9 Plant Biology in Uppsala, SE-750 07, Uppsala, Sweden

10 ²Laboratoire Reproduction et Développement des Plantes, Université de Lyon, ENS de Lyon, UCB
11 Lyon 1, CNRS, INRA, INRIA, Lyon 69007, France

12 ³Experimental Biology Research Group, Institute of Biology, Faculty of Sciences, University of
13 Neuchâtel, 2000 Neuchâtel, Switzerland

14 ⁴Institut Jean-Pierre Bourgin, INRAE, AgroParisTech, Université Paris-Saclay, 78000 Versailles, France

15 ⁵Department of Plant Sciences, University of Cambridge, Downing Street, Cambridge CB2 3EA, UK

16 ⁶Université Paris-Saclay, CNRS, INRAE, Univ Evry, Institute of Plant Sciences Paris-Saclay (IPS2),
17 91405 Orsay, France.

18 ⁷Université de Paris, CNRS, INRAE, Institute of Plant Sciences Paris-Saclay (IPS2), 91405, Orsay,
19 France

20

21 *Correspondence : yoan.coudert@ens-lyon.fr

22 **Abstract**

23 Shoot branching mechanisms where branches arise in association with leaves – referred to
24 as lateral or axillary branching – evolved by convergence in the sporophyte of vascular plants
25 and the gametophyte of bryophytes, and accompanied independent events of plant
26 architectural diversification¹. Previously, we showed that three hormonal cues, including
27 auxin, have been recruited independently to co-ordinate branch patterning in flowering plant
28 leafy shoots and moss gametophores (Coudert, Palubicki *et al.*, 2015)²⁻⁴. Moreover, auxin-
29 mediated apical dominance, which relies on local auxin production, has been proposed as a
30 unifying molecular regulatory mechanism of branch development across land plants⁵. Whilst
31 our previous work in the moss *Physcomitrium patens* has gathered indirect evidence
32 supporting the notion that auxin synthesized in gametophore apices regulates branch
33 formation at a distance², direct genetic evidence for a role of auxin biosynthesis in
34 gametophore branching control is still lacking. Here, we show that gametophore apex
35 decapitation promotes branch emergence through massive and rapid transcriptional
36 reprogramming of auxin-responsive genes and altering auxin biosynthesis gene activity.
37 Specifically, we identify a subset of *P. patens* *TRYPTOPHAN AMINO-TRANSFERASE (TAR)*
38 and *YUCCA FLAVIN MONOOXYGENASE-LIKE (YUC)* auxin biosynthesis genes expressed in
39 apical and basal regions of the gametophore, and show that they are essential for branch
40 initiation and outgrowth control. Our results demonstrate that local auxin biosynthesis
41 coordinates branch patterning in moss and thus constitutes a shared and ancient feature of
42 shoot architecture control in land plants.

43 **Introduction**

44 Understanding the mechanisms that determine the shape of living organisms is a central goal
45 of biology. In plants, branching patterns are a major determinant of shape diversity^{6,7}. Indeed,
46 most plant shoots have the capacity to develop indeterminately, which allows for the
47 continuous production of new growth axes, or branches, throughout their lifetime⁷. Apical
48 dominance, the inhibitory effect exerted by shoot apices on the initiation or outgrowth of
49 distant lateral buds, is a fundamental regulatory mechanism of branching form development.
50 It was first described in vascular plants and is mediated, at least partly, by the production of
51 the phytohormone auxin at the dominant shoot apex^{3,8}. Studies in mosses have shown that
52 excision of the gametophore (*i.e.* the gametophytic leafy shoot) tip – referred to as
53 decapitation – triggers *de novo* branch formation^{2,9}, indicating that apical dominance is
54 conserved beyond vascular plants. Using the moss *Physcomitrium patens* as a model, we
55 have shown that decapitation-induced branching can be alleviated by the application of
56 auxin-impregnated lanolin on the stump of decapitated gametophores². We have further
57 demonstrated the inhibitory effect of auxin on branch formation by quantifying the branching
58 patterns of *P. patens short internodes 2-1 (shi2-1)* mutants that lack a putative transcriptional
59 regulator of *YUCCA FLAVIN MONOOXYGENASE-LIKE (YUC)* auxin biosynthesis genes^{10,11},
60 *SHI1* over-expressors and wild-type gametophores treated with natural and synthetic auxins².
61 We have also used a computational modelling approach to investigate whether a regulatory
62 mechanism of branch initiation by auxin-mediated apical dominance could account for
63 observed branch distribution patterns in wild-type and mutant gametophores². Whilst our
64 model supports the notion that local auxin production in the main gametophore apex and
65 branch apices patterns branch formation at the whole-shoot level, direct genetic evidence
66 for local auxin production in branch apices is lacking and a role for auxin biosynthesis genes
67 in the regulation of gametophore branching has not been demonstrated yet. More generally,
68 the relative contribution of auxin to gametophore branching is poorly understood and non-
69 hormonal regulatory mechanisms are yet to be identified. In this study, we took advantage of
70 the possibility to trigger branch formation by gametophore decapitation in the moss *P. patens*
71 to address these fundamental biological questions.

72

73 **Results**

74 **Massive and rapid reprogramming of early auxin-responsive genes follows** 75 **gametophore decapitation**

76 To first assess the dynamics of branch emergence following decapitation, we isolated
77 gametophores from 4-week-old wild-type colonies, cut off their apices and followed the

78 development of branches over 48 hours. The first emerged branches were clearly visible 24
79 hours after decapitation (h.a.d.) and branches with well-developed leaves could be observed
80 48 h.a.d., suggesting that the earliest molecular events leading to branching occur within a
81 day (Figure 1A). To capture a comprehensive overview of the transcriptional changes
82 associated with early branch development, we next analyzed the transcriptome of whole
83 gametophores collected 2, 6, 12 and 24 h.a.d., and used gametophores collected
84 immediately after decapitation (0 h.a.d.) as a reference. The proportion of genes whose
85 transcription was affected increased up to 12 h.a.d., leading to a maximum of 5028 and 4734
86 genes down- and up-regulated, respectively, suggesting that major transcriptional changes
87 occur before the first branches become visible (Table S1, Figure S1 and S2). Gene ontology
88 (GO) term analyses identified distinct enriched functional categories in both datasets (Table
89 S2), but auxin-related GO terms were not significantly enriched, which was unexpected as
90 published data suggest an important role for auxin in gametophore branching control². To
91 specifically address the contribution of auxin in decapitation-induced branching, we sought
92 to directly compare the effect of auxin and decapitation at the transcriptional level. To this
93 end, we sequenced the transcriptome of 4-week-old wild-type gametophores treated with
94 indole-3-acetic-acid (IAA) for a short time period (30 min) and used mock-treated plants as a
95 reference to identify early auxin-responsive genes. We found that 3652 and 4524 genes were
96 down- and up-regulated by IAA, respectively (Table S1). By cross-referencing decapitation
97 and IAA-regulated gene sets, we observed a striking anti-correlation between both
98 treatments (Figure 1B). Sixty-four percent of genes down-regulated 2 h.a.d. were IAA-
99 induced, whilst only 5% were IAA-repressed. A similar trend was observed for “6 h.a.d.” (IAA-
100 induced genes, 61% ; IAA-repressed genes, 6%) and “12 h.a.d.” (IAA-induced genes, 51% ;
101 IAA-repressed genes, 8%) gene sets. For example, both *ARF* and *AUX/IAA* auxin signalling
102 genes, previously identified as early auxin-responsive genes¹², responded oppositely in that
103 all the genes but one were induced by IAA and repressed after decapitation (Figure 1C).
104 Inversely, 46% of genes up-regulated 2 h.a.d. were IAA-repressed, whilst only 14% were
105 IAA-induced, with a similar trend for “6 h.a.d.” (IAA-repressed genes, 49% ; IAA-induced
106 genes, 8%) and “12 h.a.d.” (IAA-repressed genes, 34% ; IAA-induced genes, 11%) gene
107 sets (Figure 1B). Thus, the opposite effect of decapitation and auxin application on the overall
108 gametophore transcriptional response support the notion that the main gametophore apex
109 is a major auxin source. Taken together, our data indicate that early auxin-responsive genes
110 play a major role in the decapitation response.

111

112 **Decapitation rapidly alters *TAR* and *YUC* auxin biosynthesis gene expression**

113 We reasoned that our dataset would provide a reference to identify genes controlling apical
114 dominance, both in an auxin-dependent and independent manner (see Discussion). In this
115 context, we sought to test further the hypothesis that gametophore apices are sites of auxin
116 biosynthesis. Auxin is derived from tryptophan (TRP)-independent and dependent
117 biosynthetic pathways¹³. In the latter, the dominant pathway in plants, TRP is converted to
118 indole-3-pyruvic acid (IPyA) by TRYPTOPHAN AMINO-TRANSFERASE (TAA/TAR) enzymes,
119 that is then converted to auxin by YUCCA FLAVIN MONOOXYGENASE-LIKE (YUC)
120 enzymes¹⁴⁻¹⁷. Auxin metabolite profiling in *PpTAR* and *PpYUC* overexpression lines, and
121 *pptar* mutants have suggested that both steps of auxin biosynthesis are essential and
122 identified TRP-to-IPyA conversion as a rate-limiting step in *P. patens*^{13,18,19}. To determine the
123 changes in auxin biosynthesis gene activity during decapitation-induced branching, we
124 therefore retrieved *PpTAR* (named *TAR* hereafter for the sake of readability) and *PpYUC*
125 (named *YUC* hereafter) expression profiles from our RNA-seq data. We identified two *TAR*
126 and three *YUC* genes significantly differentially expressed after decapitation (Figure 1D and
127 1E). Specifically, *TARA* (*Pp3c21_15370V3.1*), *TARC* (*Pp3c17_6500V3.1*) and *YUCF*
128 (*Pp3c3_20490V3.1*) were induced as early as 2 h.a.d., *YUCC* (*Pp3c1_11500V3.1*) was
129 induced from 12 h.a.d., and *YUCB* (*Pp3c11_11790V3.1*) was repressed. We also found that
130 the expression of *TARA*, *YUCE* (*Pp3c13_21970V3.1*) and *YUCF*, but not *TARC*, *YUCB* and
131 *YUCC*, was affected by exogenous auxin, suggesting that auxin may to some extent regulate
132 its own biosynthesis.

133

134 ***TAR* and *YUC* genes are active in the tip, branch apices and basal portion of** 135 **gametophores**

136 To determine the expression domain of *TARA*, *TARC*, *YUCB*, *YUCC* and *YUCF* genes, we
137 analysed the activity of transcriptional fusions between corresponding promoter regions and
138 a GFP-GUS chimeric protein transformed in a wild-type background (Figure S3). Two to three
139 independent transgenic lines were observed for each genetic construct (Table S4). We found
140 that the spatial expression domains of *TAR* and *YUC* promoters largely overlapped in whole
141 gametophores. Beta-glucuronidase (GUS) activity was detected at the main apex, at the base,
142 notably in rhizoid cells, and in discrete regions of the stem corresponding to initiating branch
143 apices (Figure 2A, 2D, 2G, 2J and 2M). At the main apex, *TAR* promoter activity was observed
144 in the apical cell and emerging leaves, as reported previously¹⁸, and both *TAR* and *YUC*
145 promoters were highly active in axillary hair cells surrounding the gametophore apical cell,
146 reminiscent of the expression pattern of other auxin-related genes like *PpSHI1* and *PpSHI2*¹⁰
147 (Figure 2P and 2Q). Promoter activity of *YUCF*, and to a lesser extent *YUCB* and *YUCC*, was

148 also detected in axillary hair cells elsewhere on the stem (Figure 2M, 2R). This indicates that
149 the expression of *TARA* and *TARC* is more restricted in space than that of *YUCB*, *YUCC* and
150 *YUCF*, and it is therefore unlikely that auxin biosynthesis occurs in leaf axils in the absence
151 of *TARA* or *TARC* activity.

152 To determine how decapitation affected the activity of selected *TAR* and *YUC* transcriptional
153 reporters, gametophores were collected 24 hours after apex excision and stained for GUS
154 activity, thereby leaving enough time for new branches to initiate and grow out. The intensity
155 of GUS accumulation patterns remained overall similar to intact controls, except for the
156 *YUCB* promoter that seemed more weakly expressed after decapitation, likely reflecting its
157 transcriptional repression (Figure 1E). The spatial distribution of these patterns was changed
158 in leaf axils where we observed an activation of *TARA*, *TARC*, *YUCB*, *YUCC* and *YUCF*
159 expression associated with the formation of new branches. The activity of *TARA* and *TARC*
160 promoters was detected from the earliest stage of branch formation, throughout the branch
161 initium (Figures 2B, 2C, 2E and 2F). In contrast, *YUCB*, *YUCC* and *YUCF* promoter activity
162 were first detected at a later stage when the first leaves were clearly visible, and mostly in
163 hair cells of the branch apical region (Figures 2H, 2I, 2K). At a more mature stage of branch
164 development, *i.e.* when leaves and brown rhizoids were well-developed, *TARA*, *TARC*, *YUCB*,
165 *YUCC* and *YUCF* genes were active in overlapping spatial domains mirroring those described
166 previously in whole gametophores (Figures 2I, 2L and 2O, data not shown for *TARA* and
167 *TARC*). The temporal delay between *TAR* and *YUC* gene activation and the differences in
168 their spatial expression domains at early stages of branch initiation suggest that IPyA might
169 be transported from the meristematic cells where it is synthesized to adjacent hair cells to be
170 converted to auxin by *YUC* enzymes. Alternatively, these differences might be explained by
171 the short-range movement of *TAR* or *YUC* mRNA, or corresponding proteins; the involvement
172 of *YUC* genes co-expressed with *TARA* and *TARC* but not differentially expressed in our
173 RNA-seq dataset, such as *YUCE* (Figure S4); or unmask a putative *YUC*-independent
174 function of IPyA. Together, the above data suggest that TRP-dependent auxin biosynthesis
175 occurs primarily in the main apex and the basal portion of gametophores, and resumes locally
176 in leaf axils when new branches initiate.

177

178 ***TAR* genes prevent systematic branch initiation**

179 To investigate the function of *TARA* and *TARC* genes in gametophore branching, we grew
180 *tara*, *tarc* and *tarac* knock-out mutants¹⁸ for 5 or 7 weeks and quantified their branching
181 patterns, as done previously². We found that *tara* single mutants had similar phenotypes to
182 wild-type control plants. There was moderate evidence²⁰ that *tarc* branch density was lower

183 than control plants in older gametophores, indicating that *tarc* single mutants were also very
184 similar to wild-type (Figures 3A-3C, 3E-3G and 3K-3N). In contrast, there was strong
185 evidence that *tarac* double mutants had a shorter apical inhibition zone and inter-branch
186 distance, and an increased branch density with respect to wild-type plants, suggesting a
187 reduced apical dominance and lateral inhibition from branch meristems (Figure 3D, 3H, 3K,
188 3L and 3O). We also observed that the position of the lowermost branch was closer to the
189 gametophore base in *tarac* mutants than in wild-type (Figure 3P), and the number of branches
190 in the three most basal metamers was much higher in *tarac* mutants (n = 23 branches) than
191 in *tara* (n = 2), *tarc* (n = 2) or wild-type (n = 5) gametophores, suggesting that local *TAR* activity
192 prevents branching at the gametophore base (Figures 3A-3D). Despite the overall increase in
193 branch number in *tarac* mutants, we observed strong disparities in the branch distribution
194 pattern between gametophores. Whilst some gametophores bore branches on up to six
195 consecutive metamers (see gametophore #1 in Figure 3D), which has never been reported
196 elsewhere before, others had few or no visible branches at all, which was rather counter-
197 intuitive (Figure 3D). However, on closer inspection of *tarac* gametophores, we noticed that
198 tiny buds were nested in nearly every single leaf axil lacking a visible branch (Figure 3I-3J).
199 This suggests that branch initiation was almost systematically de-repressed in *tarac* mutants
200 while subsequent outgrowth was inhibited. Consistent with observed *TARA* and *TARC*
201 expression patterns in whole gametophores and emerging branches, our data indicate that
202 both genes act redundantly in the apices and basal portion of gametophores and their activity
203 is necessary to prevent branch initiation and co-ordinate branch patterning.

204

205 ***YUC* genes suppress branching**

206 Then, to determine the role of decapitation-induced *YUC* genes in gametophore branching,
207 we grew *yucc*, *yucf* and *yuccf* knock-out mutants¹⁸ for 5 or 7 weeks and quantified their
208 branching patterns² (Figure S5). Whilst the apical inhibition zone size was increased in *yucc*
209 gametophores, the distance to the closest branch, the position of the lowermost branch of
210 *yucc* and *yucf* gametophores were not changed with respect to wild-type controls (Figure
211 4A-4C, 4E-4G, 4I-4M). We observed slight perturbations of the branch distribution patterns
212 in *yucc* and *yucf* single mutants, mostly explained by the branching patterns of older
213 gametophores (Fig 4L-M). In contrast, we found strong evidence that *yuccf* double mutants
214 had a reduced apical inhibition zone and inter-branch distance, and moderate evidence of
215 an increased branch density with respect to wild-type plants (Figure 4D, 4H, 4I-4K, 4N).
216 Moreover, the position of the lowermost branch was closer to the gametophore base in *yuccf*
217 double mutants than in wild-type (Figure 3P), and the number of branches in the three most

218 basal metamers was higher in *yuccf* mutants (n = 15 branches) than in *yucc* (n = 11), *yucf* (n
219 = 6) or wild-type (n = 3) gametophores. Unlike *tarac* mutants, we did not observe emerging
220 buds in the leaf axils of *yuccf* gametophores. However, we sometimes noticed
221 supernumerary branches growing from the base of lateral branches in *yucc* mutants,
222 consistent with *YUCC* expression at the base of branches (Figure 4F) and indicating a local
223 inhibitory effect of *YUCC*. Moreover, branches seemed less developed in both single and
224 double *yuc* mutants than in wild-type plants. Together, the above data coincide with
225 observed expression patterns of *YUC* transcriptional reporters and indicate that *YUCC* and
226 *YUCF* act redundantly to inhibit branch formation but promote subsequent growth, hence
227 supporting the hypothesis of a local role of auxin biosynthesis in branch patterning.

228

229 **Discussion**

230 This work primarily aimed to determine the relative importance of auxin in gametophore
231 branching and test the hypothesis that apically synthesized auxin patterns branch distribution.
232 Using an RNA-seq approach, we show that early auxin-responsive genes have a major
233 contribution to the transcriptional response of gametophores to decapitation. We also
234 provide evidence that several *TAR* and *YUC* genes, together responsible for the enzymatic
235 conversion of tryptophan to auxin, are active in the main apex and branch apices, and the
236 base of gametophores^{13,18}, and identify a prominent and dual role for *TARA* and *TARC* in
237 branch initiation and growth. First, our data show that apical auxin sources suppress branch
238 initiation at a distance. Indeed, observed perturbations of branching patterns in *tarac* and
239 *yuccf* mutants (*i.e.* the reduction of the apical inhibition zone size and distance between
240 closest branches, and the increase of branch density) qualitatively match the predicted
241 outcome of our published computational model of gametophore branching control by
242 hormonal cues where a reduction of auxin production in the main and lateral apices promotes
243 branching². Interestingly, the model has also identified that a basal inhibitory cue is locally
244 required to prevent branching, and genetic experiments previously led us to propose that this
245 cue is a *CCD8*-derived molecule belonging to the strigolactone family of compounds².
246 Expression patterns of selected *TAR* and *YUC* transcriptional reporters indicate that auxin
247 biosynthesis occurs in this region, and basal branching is strongly increased in *tarac* and
248 *yuccf* double mutant gametophores, suggesting that auxin may act concomitantly with the
249 *CCD8*-derived cue to fulfil this inhibitory role. Determining whether and how these two
250 hormonal cues interact will require further investigation. Second, our data indicate that an
251 adequate level of *TAR* and *YUC* activity at branch initiation sites is essential to drive branch
252 outgrowth. Branches were noticeably shorter in *tarac* mutants, and likely also in *yuccf*

253 mutants, than in wild-type. These observations corroborate the finding that *tarac*
254 gametophores have stunted growth¹⁸ and suggest that low auxin biosynthesis in
255 gametophore apices hinders apical cell proliferative activity. It has previously been reported
256 that excessive auxin accumulation in gametophore tissues may also disrupt apical cell
257 function and suppress phyllid (*i.e.* the gametophytic leaf) emergence at the apex²¹, which
258 supports the idea that cellular auxin homeostasis must be tightly controlled to ensure proper
259 gametophore growth. Third, despite two whole-genome duplications in *P. patens* and their
260 possible consequences on gene redundancy²², it must be stressed that deleting only 2 out
261 of 4 *TARs*, and 2 out of 6 *YUCs* was sufficient to reveal the function of both gene families in
262 gametophore branching control. Nevertheless, it cannot be excluded that other *TAR* or *YUC*
263 genes may also be involved in this process.

264 From an evolutionary perspective, *TAR*-*YUC*-mediated auxin biosynthesis originated in
265 streptophyte algae and is conserved in land plants^{23,24}. The genome of the liverwort
266 *Marchantia polymorpha* contains only one functional *TAA* gene, named *MpTAA*, and two *YUC*
267 genes, named *MpYUC1* and *MpYUC2*²⁵. Similar to our observations in moss gametophores,
268 *MpYUC2* expression domain is broader than that of *MpTAA* in the liverwort thallus (*i.e.* the
269 gametophytic body), and both domains overlap in meristematic notches that contain the
270 apical stem cells at the origin of thallus tissues. Although thallus branching occurs by notch
271 dichotomy, a type of apical branching that is developmentally distinct from gametophore
272 branching^{7,26}, *Marchantia taa* and *yuc* knock-down plants also display hyperbranching
273 phenotypes. Beyond bryophytes, various studies in the flowering plant *Arabidopsis thaliana*
274 have shown that *AtTAA1/WEI8*, *AtTAR2*, *AtYUC1*, *AtYUC4* and *AtYUC6* genes are expressed
275 in discrete and partially overlapping domains of the shoot apical meristem^{14,15}. Double and
276 triple mutants in these genes, including *yuc1yuc4*, *yuc1yuc4yuc6* and *taa1tar2* allele
277 combinations, show various degrees of decreased apical dominance reflected by an
278 enhanced production of branches. Together, this suggests that lateral and apical branching
279 modes evolving separately in flowering plant sporophytes, and moss and liverwort
280 gametophytes, are underpinned by a shared and ancient molecular mechanism driving local
281 auxin biosynthesis in shoot meristematic structures, which represents a novel discovery of
282 deep homology in land plants^{21,27,28}.

283 The functional analysis of *PpTAR* and *PpYUC* auxin biosynthesis genes demonstrated that
284 our RNA-seq approach has the potential to identify novel regulators of gametophore
285 branching. Moreover, the relatively small differences in gene expression detected at the
286 whole gametophore level (see for example Figure 1D-E) likely under-estimate the magnitude
287 of regulatory changes occurring locally, since genes underpinning branch initiation are

288 expressed in restricted spatial domains. In the future, our dataset will help us to decipher
289 how auxin is integrated at the molecular level to regulate branching. For instance, GO
290 analyses revealed a significant enrichment of the “DNA binding transcription factor activity”
291 term in gene sets up- and down-regulated after decapitation (Table S2). Members of the
292 *APETALA2/ETHYLENE RESPONSIVE FACTOR (AP2/ERF)* family represented about two
293 thirds of identified DNA binding transcription factor coding genes and included putative
294 conserved regulators of meristematic function, such as *STEMIN1 (Pp3c1_27440v3.1)*, known
295 to promote stem cell formation through local depletion of a repressive chromatin mark, and
296 *Pp3c26_9880v3.1*, the closest homologue to *Solanum lycopersicum LEAFLESS* and *A.*
297 *thaliana PUCHI* and *DORNRÖSCHEN-LIKE*, which are regulated by auxin and involved in
298 meristem identity and lateral organ initiation control^{29–32}. We also found that GO terms related
299 to “trehalose metabolism” were significantly enriched in the “up-regulated 2 h.a.d.” gene set.
300 Interestingly, trehalose 6-phosphate (T6P) metabolic genes regulate branching and apical
301 dominance in flowering plants^{33–35}. For example, shoot decapitation in *Pisum sativum* (pea)
302 triggers an increase of T6P levels in a few hours, which contributes to promoting branch
303 outgrowth³³. T6P is synthesized from uridine diphosphate-glucose and glucose-6-phosphate
304 by the activity of T6P SYNTHASES (TPS) and converted to trehalose by T6P
305 PHOSPHATASES (TPP), which is then hydrolysed into glucose by TREHALASES (TRE).
306 Transgenic *Arabidopsis thaliana* plants with increased TPP activity in axillary buds have
307 reduced T6P levels and delayed branch outgrowth, whilst plants with increased levels of T6P
308 in the vasculature have enhanced branching³⁴. Moreover, mutations in *Zea mays RAMOSA3*
309 (*RA3*) and its paralog *ZmTPP4* that both encode TPP enzymes, lead to increased
310 inflorescence branching^{35,36}. In *Physcomitrium*, we found that all *PpTPS* genes were
311 repressed after decapitation, whilst *PpTPP* and *PpTRE* genes were either repressed or
312 induced (Figure S6), suggesting that T6P levels are dynamically regulated during
313 decapitation-induced branching. Besides, we found that *TPS* genes were IAA-induced and
314 decapitation-repressed, and GO terms related to trehalose metabolism were associated with
315 genes both induced by auxin and up-regulated after decapitation (Table S3), consistent with
316 *TPP* and *TRE* expression profiles 2 and 6 h.a.d. (Figure S6). This suggests that apically-
317 produced auxin regulates the activity of T6P metabolic genes in the gametophore, which has
318 not been evidenced yet in flowering plants. Further studies will be needed to determine the
319 biological function of T6P metabolic genes and AP2/ERF DNA-binding transcription factors,
320 and explore their crosstalk with auxin in the moss *P. patens*. Finally, it must be stressed that
321 our dataset contains a large number of differentially expressed genes with uncharacterized

322 function, representing an untapped reservoir of novel putative regulators of shoot
323 architecture.

324

325

326 **Material and methods**

327 ***Physcomitrium patens* plant growth and transformation**

328 The Reute³⁷ strain of *Physcomitrella patens* was used as the wild-type (WT) background for
329 generating all the transgenic lines, the Gransden strain being largely sterile in laboratory
330 conditions. Moss colonies were initiated from 1 mm² spot cultures and cultivated in sterile
331 Magenta GA-7 tissue culture vessels (Bioworld, Dublin, OH, USA) on BCDAT medium (250
332 mg/L MgSO₄·7H₂O, 250 mg/L KH₂PO₄ (pH 6.5), 1010 mg/L KNO₃, 12.5 mg/L, FeSO₄·7H₂O,
333 0.001% Trace Element Solution (0.614 mg/L H₃BO₃, 0.055 mg/L AlK(SO₄)₂·12H₂O, 0.055
334 mg/L CuSO₄·5H₂O, 0.028 mg/L KBr, 0.028 mg/L LiCl, 0.389 mg/L MnCl₂·4H₂O, 0.055 mg/L
335 CoCl₂·6H₂O, 0.055 mg/L ZnSO₄·7H₂O, 0.028 mg/L KI and 0.028 mg/L SnCl₂·2H₂O), 0.92 g/L
336 di-ammonium tartrate (C₄H₁₂N₂O₆) and 8 g/L agar with CaCl₂ added to a 1 mM concentration
337 after autoclaving, at 23°C under a 16h light/8h dark cycle, at 50-150 μmol.m⁻².s⁻¹ in MLR-352
338 growth cabinets (PHCbi, Etten-Leur, The Netherlands).

339

340 **Decapitation and auxin treatment**

341 For pharmacological treatments, a 70% ethanol solution containing 100 mM indole-3-acetic
342 acid (IAA) (Merck KGaA, Darmstadt, Germany) was diluted 10,000 times in water to reach a
343 final concentration of 10 μM IAA. A 70% ethanol solution was diluted 10,000 times in water
344 and used as a mock control. Moss cultures were soaked in diluted solutions for 30 minutes
345 before tissue harvest. For decapitation, gametophores were teased apart from moss colonies
346 with thin tip tweezers, planted in an upright position on BCDAT petri dishes and their apical
347 portion was cut off with micro-scissors, as described in Coudert, Palubicki *et al.* (2015)².

348

349 **Generation of *YUC* transcriptional reporters and *yuc* mutants**

350 All the transgenic lines used in this study are listed in Table S4. Generation and confirmation
351 of the transcriptional reporter lines *TARA::GFP-GUS*, *TARC::GFP-GUS*, and *YUCF::GFP-*
352 *GUS*, as well as the knockout lines *tara*, *tarc*, *tarac*, *yucc*, and *yucf* have been previously
353 described¹⁸. To produce the *YUCB::GFP-GUS* reporter construct pMT244 (Figure S3), a 2090
354 bp *YUCB* promoter fragment was amplified from gDNA with primers SS235/SS236 and
355 trimmed with *Bam*HI/*Nco*I. The resulting fragment was cloned between the *Bam*HI/*Nco*I sites
356 of pMT211, a vector allowing promoters to be cloned ahead of a GFP-GUS reporter gene for

357 subsequent integration into the neutral *Pp108* locus³⁸. Similarly, to produce the
358 *YUCC::GFPGUS* reporter construct pMT251 (Figure S3), a 1767 bp *YUCC* promoter fragment
359 was amplified from gDNA with primers SS237/SS238, trimmed with *Bam*HI/*Bsp*HI, and
360 cloned between the same two sites in pMT211. Both reporter constructs were linearized with
361 *Sfi*I before they were transformed into WT protoplast as previously described³⁹. Stable
362 transformants were selected in the presence of 50 µg.ml⁻¹ hygromycin (Duchefa H0192;
363 Haarlem, the Netherlands). Correct integration was confirmed by PCR (Figure S3). For primer
364 sequences, see Table S5. The *yuccf* double knockout lines were produced by a sexual cross
365 of the confirmed single mutants *Ppyucc-2* and *Ppyucf-1* described previously¹⁸, according to
366 the method presented in Thelander *et al.*³⁸. Double knockout lines were confirmed by PCRs
367 demonstrating the loss of internal gene sequences (Figure S5).

368

369 **GUS staining and plant imaging**

370 *Physcomitrium patens* gametophores were isolated from colonies grown on BCDAT and
371 incubated at 37°C in a 100 mM phosphate buffer (pH 7) with 10 mM Tris (pH 8), 1 mM EDTA
372 (pH 8), 0.05% Triton X-100, 5mM potassium ferricyanide, 5mM potassium ferrocyanide and
373 2 mM X-GlcA (5-Bromo-4-chloro-3-indolyl-β-D-glucuronic acid), using times indicated in
374 Figure 2. Tissues were de-stained in 70% ethanol and imaged with a Keyence VHX-900F
375 digital microscope with a 5-50 X or a 50-200 X objective. Plants not subject to GUS staining
376 were imaged in the same conditions.

377

378 **Definition of branches in *Physcomitrium patens***

379 According to Coudert *et al.*¹, a module is defined as “a portion of gametophore arising from
380 a single apical cell”. Here, we consider that the main gametophore axis corresponds to a
381 Class I module, and gametophore branches correspond to Class II lateral modules.

382

383 **RNA-seq data production and analysis**

384 For each biological replicate and condition, RNA were pooled from 5-10 gametophores
385 (Gransden⁴⁰ strain). Three independent biological replicates were produced. Total RNA was
386 extracted using an RNeasy Plant Mini Kit (Qiagen, Hilden, Germany) and treated with DNase
387 according to the supplier’s instructions. RNA-seq libraries were made using the
388 TruSeq_Stranded_mRNA_SamplePrep_Guide_15031047_D protocol (Illumina, California,
389 U.S.A.). The RNA-seq samples have been sequenced in paired-end (PE) with a sizing of 260
390 bp and a read length of 75 bases, using an Illumina NexSeq500 technology (IPS2, POPS
391 platform, Gif-sur-Yvette). 24 samples were processed by lane of NextSeq500 using individual

392 bar-coded adapters, generating approximately 30 millions of PE reads per sample. All
393 experimental steps, from growth conditions to bioinformatic analyses, were deposited in the
394 CATdb database⁴¹ (<http://tools.ips2.u-psud.fr/CATdb/>, ProjectID NGS2017_09_Moss1)
395 according to the MINSEQE ‘minimum information about a high-throughput sequencing
396 experiment’ (<https://doi.org/10.25504/FAIRsharing.a55z32>). To facilitate comparisons, all
397 samples were processed similarly from trimming to count. RNA-Seq pre-processing included
398 trimming library adapters and performing quality controls. Raw data (fastq) were trimmed
399 with fastx toolkit for Phred Quality Score Qscore >20, read length >30 bases, and ribosome
400 sequences were removed with sortMeRNA⁴². The mapper Bowtie⁴³ (version 2) was used to
401 align reads against the *Physcomitrium (Physcomitrella) patens* transcriptome (with local
402 option and other default parameters). The 32926 genes were extracted from Phytozome
403 database (*Physcomitrella patens* transcripts v3.1 gene model). The abundance of each gene
404 was calculated by a local script which parses SAM files and counts only paired-end reads for
405 which both reads map unambiguously one gene, removing multi-hits. According to these
406 rules, around 82,7% of PE reads were associated to a gene, 5-6% PE reads were unmapped
407 and 12-13% of PE reads with multi-hits were removed. Choices for the differential analysis
408 were made based on the article by Rigail *et al*⁴⁴. Genes which did not have at least one read
409 after a counts per million (CPM) normalization in at least one half of the samples were
410 discarded. Library size was normalized using the TMM method and count distribution was
411 modeled with a negative binomial generalized linear model. Dispersion was estimated by the
412 edgeR method⁴⁵ (version 1.12.0) in the statistical software ‘R’ (<http://www.R-project.org>,
413 version 2.15.0). Expression differences were compared between “0 h.a.d.” and “2 h.a.d.”, “6
414 h.a.d.”, “12 h.a.d.” or “24 h.a.d.” conditions for the “decapitation experiment”, and between
415 samples “mock” and “10 μ M IAA” conditions for the “auxin experiment”, using likelihood ratio
416 test and p-values were adjusted by the Benjamini-Hochberg procedure to control FDR. A
417 gene was considered as differentially expressed if its adjusted p-value was lower than 0.05.
418 Venn diagrams were generated using InteractiVenn⁴⁶. Gene Ontology (GO) term enrichment
419 analyses were performed with ShinyGO (version 0.66)⁴⁷.

420 **RNA-seq data availability**

421 RNA-seq datasets are available in the international repository GEO (Gene Expression
422 Omnibus⁴⁸, <http://www.ncbi.nlm.nih.gov/geo>) under the project identifier GSE188843 (token
423 = ctslsswyfjchdcp).

424

425 **Sample-size estimation and replicates**

426 For data shown in Figure 1, three independent biological replicates were produced for each
427 condition, and each replicate corresponded to RNA extracted from 5 to 10 gametophores.
428 For Figure 2, two or three independent transgenic lines were analysed for *TAR* and *YUC*
429 transcriptional reporters. Independent lines transformed with the same genetic construct
430 showed similar GUS staining patterns. Numbers in panels A, D, G, J and M indicate the
431 proportion of gametophores with a GUS staining pattern similar to the picture. For Figure 3,
432 data shown in panels A-D were obtained from 30 gametophores collected 5 weeks after
433 protonema inoculation and 30 gametophores collected 7 weeks after protonema inoculation,
434 metrics in panels K, L and P could be calculated only for gametophores with more than one
435 branch, data in panels M-O correspond to all gametophores. For Figure 4, data shown in
436 panels A-D were obtained from 30 gametophores collected 5 weeks after protonema
437 inoculation and 30 gametophores collected 7 weeks after protonema inoculation, data in
438 panels I-K could be calculated only for gametophores with more than one branch, data in
439 panels L-N correspond to all gametophores.

440

441 **Statistical analyses**

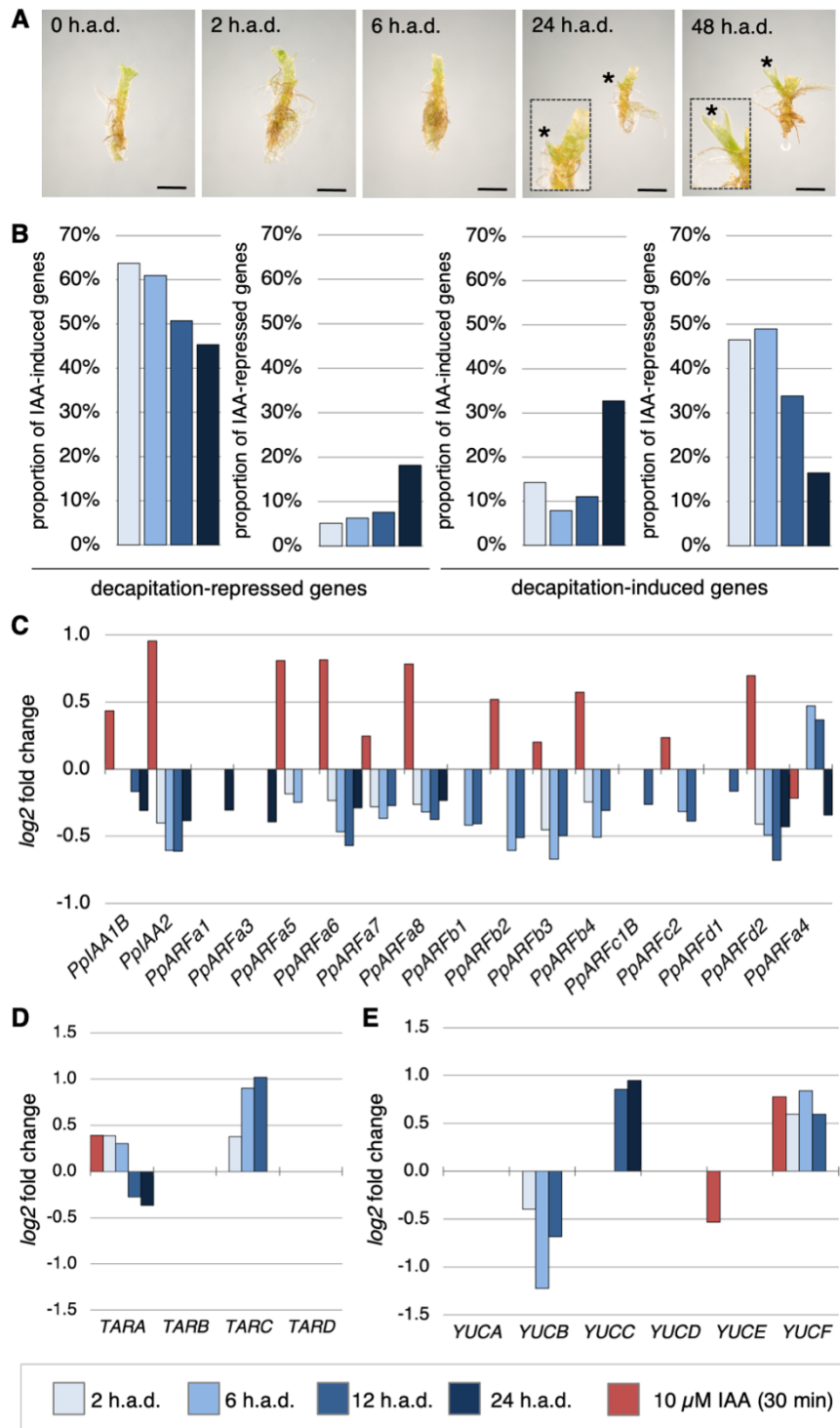
442 Generalised linear modelling was used to test whether the relationship between branch
443 number and gametophore length depended on genotype (File S1). Poisson or negative
444 binomial regression was used, depending on whether the data were over-dispersed, *i.e.*
445 whether the data were more variable than would be expected under a Poisson model. The
446 most complex fitted models were of the form $\log(\mathbb{E}(B|L, X)) = a_0 + a_1X + (a_2 + a_3X)L$, in
447 which a_0 , a_1 , a_2 and a_3 are coefficients, L is the length, X is an indicator variable depending
448 on genotype (*i.e.* X took values of either 0 or 1 depending upon whether the mutant or WT
449 was considered), and $\mathbb{E}(B|L, X)$ is the expected branch number (B) at any given pair of
450 values of L and X . Analysis of deviance and backwards stepwise elimination was used to find
451 the minimal model that received support from the experimental data. A mutant was
452 considered different from WT if either the interaction term (a_3) or the term corresponding to
453 genotype (a_1) remained in the minimal model, *i.e.* if the expected branch number was affected
454 by the value of X . The choice of whether to use a Poisson and negative binomial model was
455 made via a formal test of over-dispersion for the Poisson version of the model with an
456 interaction, using the function `overdispersion()` in the package `AER`⁴⁹. The terms “weak”,
457 “moderate”, “strong” and “very strong evidence” reflected the translation of p-values into the
458 language of evidence proposed by Muff *et al.*²⁰

459

460

461 **Figures and figure legends**

462



463

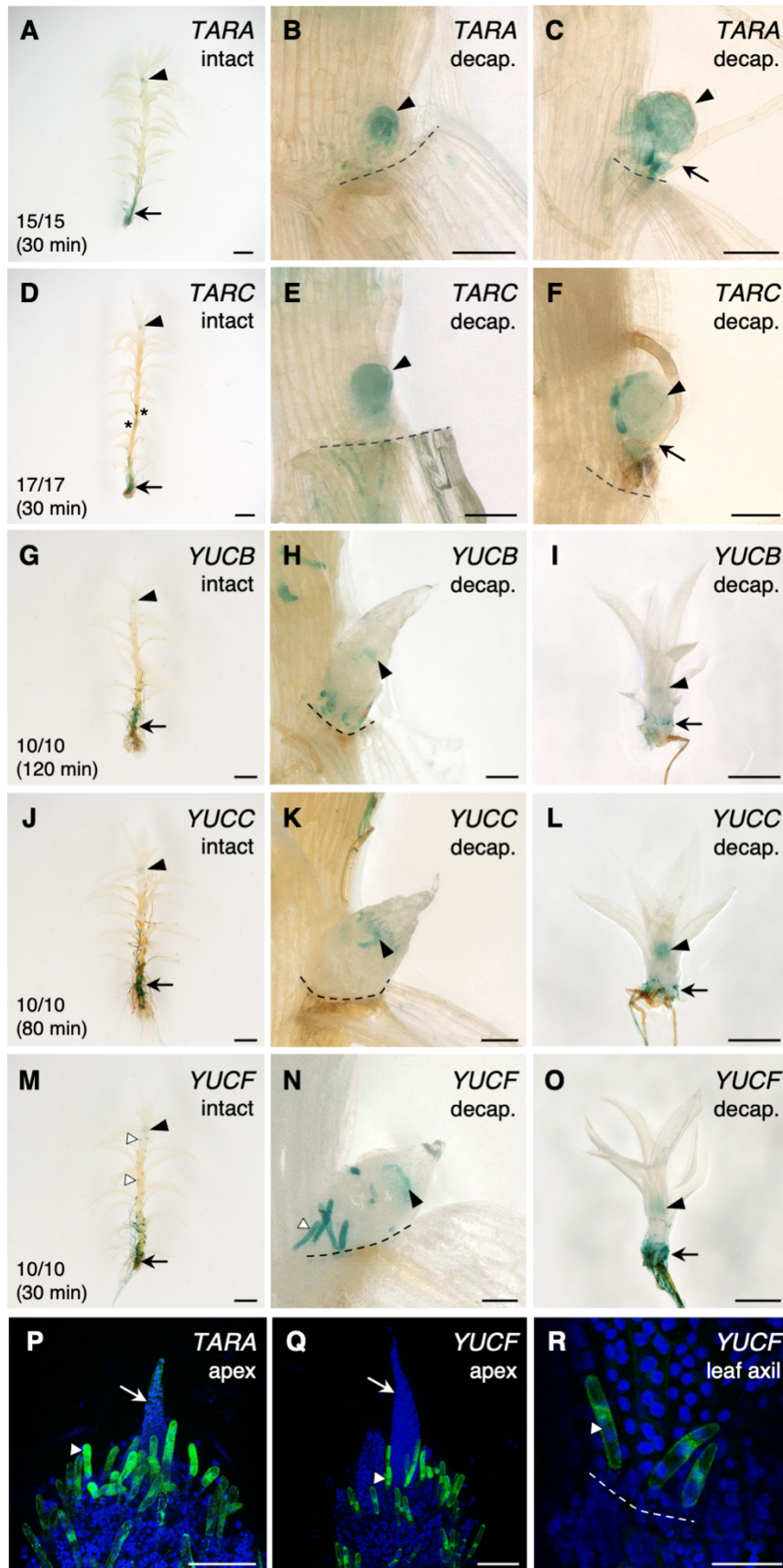
464 **Figure 1. Decapitation affects the expression of early auxin-responsive genes, and**

465 **auxin signalling and biosynthesis genes. (A) New branches (indicated with asterisks)**

466 **emerged within 24 hours after gametophore decapitation. Leaves were removed before**

467 **imaging to observe gametophore branches. Insets show magnifications of emerging**

468 branches. Scale bar = 1 mm. **(B)** Cross-analysis of transcriptomes of decapitated and auxin-
469 treated gametophores showed that about two thirds of the genes repressed 2 h.a.d. were
470 induced by a 30-minute treatment with 10 μ M indole-3-acetic acid (auxin), and conversely
471 nearly half of the genes induced 2 h.a.d. were repressed by auxin. **(C)** Bar plots showed that
472 all but one *ARF* and *AUX/IAA* auxin signalling genes identified were repressed after
473 decapitation and induced by auxin. **(D-E)** Expression of two *TAR* and three *YUC* auxin
474 biosynthesis genes was affected by decapitation. The colour code shown at the bottom of
475 the figure is used in panels B-E.
476

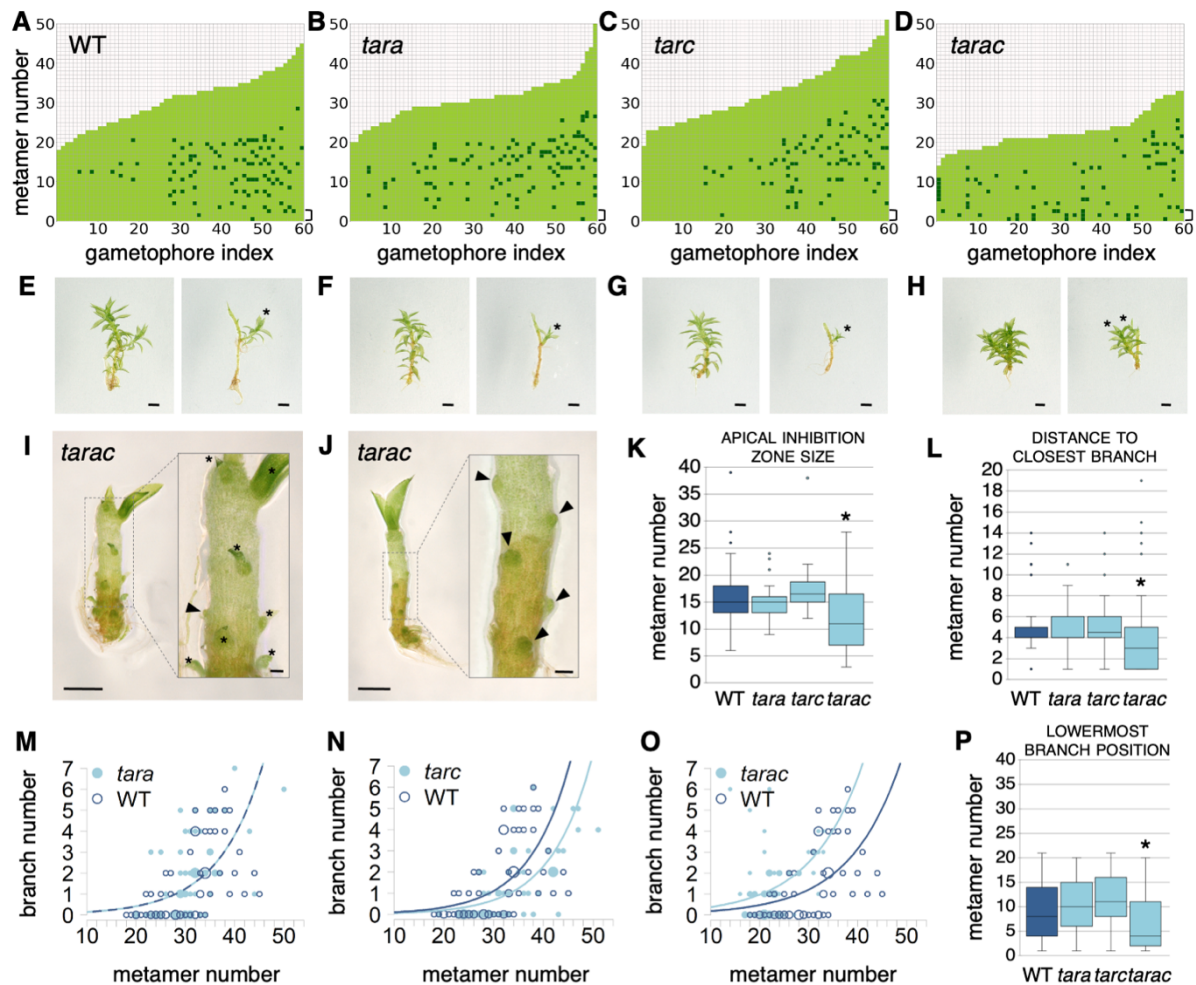


477

478 **Figure 2. *TAR* and *YUC* genes are expressed in meristematic and basal regions of**

479 ***Physcomitrium* gametophores. (A-O) GUS staining of *TARA::GFP-GUS* (A-C), *TARC::GFP-***

480 *GUS* (D-F), *YUCB::GFP-GUS* (G-I), *YUCC::GFP-GUS* (J-L) and *YUCF::GFP-GUS* (M-O)
481 transgenic lines revealed that *TAR* and *YUC* genes are active in largely overlapping
482 expression domains. Gametophores were either observed before (“intact”) or after (“decap.”)
483 apex excision. In intact gametophores, *TARA* and *TARC* are expressed in the main apex
484 (black arrowheads), in emerging branches (asterisks) and in the basal region (black arrows)
485 (A, D). Following decapitation, *TARA* and *TARC* expression is detected in initiating lateral
486 branches (black arrowheads) but not in rhizoids (black arrows) (B, C, E, F). In intact
487 gametophores, *YUCB*, *YUCC* and *YUCF* are expressed in the main apex (black arrowheads)
488 and in the basal region (black arrows). *YUCF* expression is also observed in axillary hairs in
489 leaf axils (white arrowheads) (G, J, M). Following decapitation, *YUCB*, *YUCC* and *YUCF*
490 expression is first detected at a later stage than *TARA* and *TARC*. GUS staining was found
491 in axillary hairs at the apex of newly formed branches (black arrowheads) and, at a later stage,
492 in branch rhizoids (black arrows) (H, I, K, L, N, O). (**P-R**) GFP signal in *TARA::GFP-GUS* and
493 *YUCF::GFP-GUS* lines was strongest in hairs (white arrowheads) located at the gametophore
494 apex (P-Q), and/or in leaf axils (R). Emerging leaves are indicated with white arrows. Dashed
495 lines mark the boundary between the stem and the detached leaf (B, C, E, F, H, K, N, R).
496 Gametophores were soaked in GUS staining solution for times specified in panels A, D, G, J
497 and M. The scale bars represent 1 mm in A, D, G, J and M, 500 μm in I, L, and O, 100 μm in
498 B, C, E, F, H, K, P and Q, and 50 μm in N and R.
499



500

501

502

503

504

505

506

507

508

509

510

511

512

513

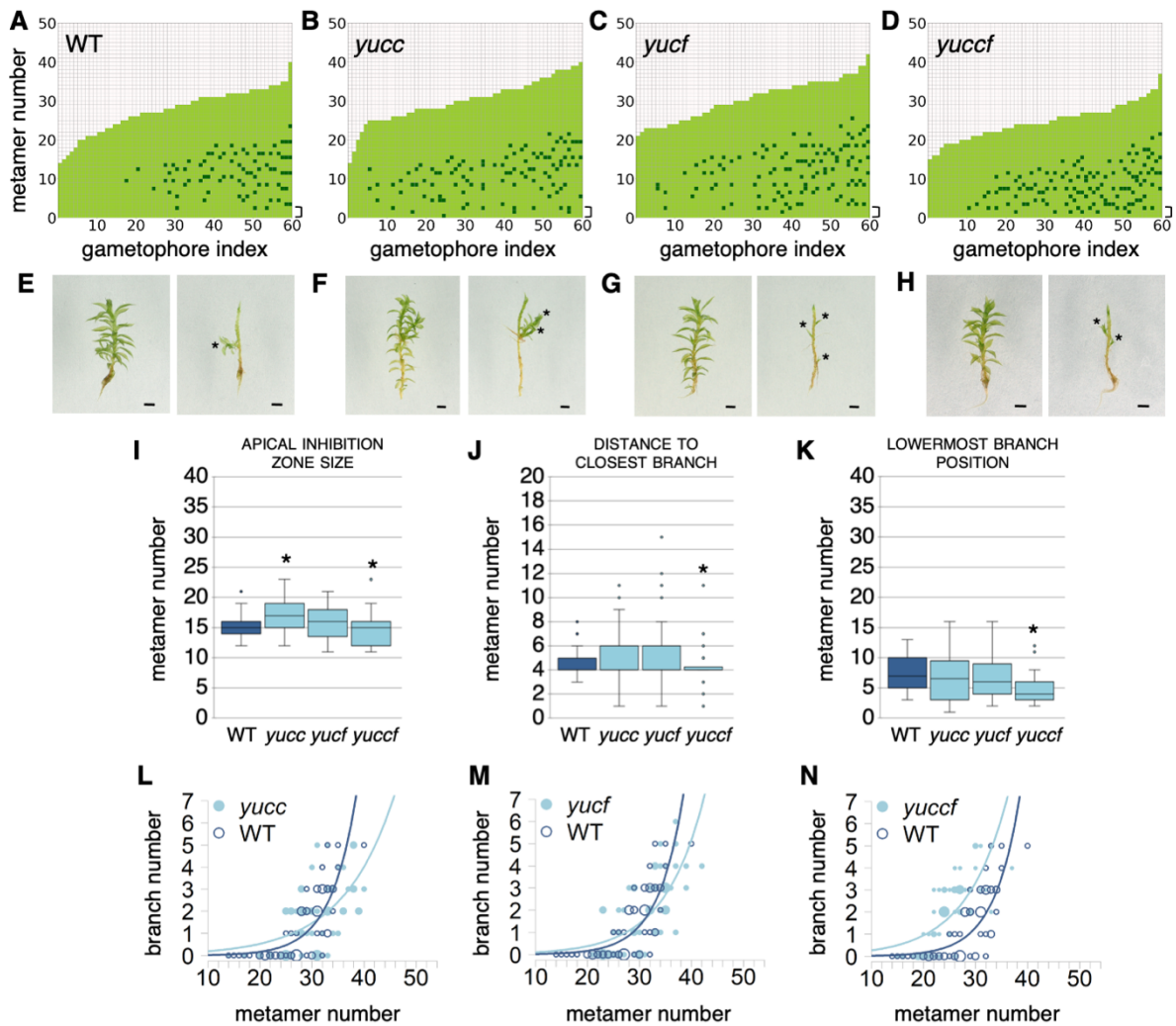
514

515

516

Figure 3. *TARA* and *TARC* genes prevent branch initiation and pattern branch distribution along the gametophore axis. (A-D) Branching patterns in WT, *tara*, *tarc* and *tarac* mutants are presented as in Coudert, Palubicki *et al.* (2015)². Brackets indicate the three lowermost metamers. (E-H) WT (E), *tara* (F), *tarc* (G) and *tarac* (H) gametophores before (left) and after (right) removing leaves, with asterisks marking branches. Scale bars represent 1 mm. (I-J) *tarac* gametophores with leaves removed revealed lateral buds with no visible leaves (arrowheads) and tiny branches with few visible leaves (asterisks), which is never observed in WT in which branches initiate *de novo* and grow out with no dormancy period. Scale bars represent 500 μ m in the main panels and 100 μ m in the insets. (K) There was strong evidence²⁰ that the apical inhibition zone was reduced in *tarac* double mutants, but not in *tara* or *tarc* single mutants, compared with wild-type control (Wilcoxon rank sum test with continuity correction different from WT, *p-value ≤ 0.05 ; WT versus *tara*, p-value = 0.35; WT versus *tarc*, p-value = 0.07; WT versus *tarac*, p-value = 0.005). (L) There was very strong evidence that the distance to the closest branch, a measurement of branch spacing, was significantly reduced in *tarac* double mutants, but not in *tara* or *tarc* single mutants, compared with wild-type control (Wilcoxon rank sum test with continuity correction different from WT,

517 *p-value ≤ 0.05 ; WT versus *tara*, p-value = 0.92 ; WT versus *tarc*, p-value = 0.14 ; WT versus
518 *tarac*, p-value = 0.0009). **(M-O)** Bubble plots showed that branch number at a given length is
519 increased in *tarac*, slightly decreased in older *tarc* gametophores, and unchanged in *tara*,
520 compared with WT. Gametophore length is represented as the number of metamers and the
521 bubble area is proportional to the number of gametophores with the same branch number
522 (B) at a given length (L). The data were over-dispersed, and so negative binomial regression
523 was used to test whether and how the relationship between branch number and
524 gametophore length differed between mutants and WT (see ‘Material and methods’). For (M)
525 the best-fitting relationship indicated no difference between *tara* and WT (p-value = 0.39;
526 $\log(\mathbb{E}(B|L)) = -3.11 + 0.11L$ for both treatments). For (N) the best-fitting relationship
527 indicated WT was larger than *tarc* at all lengths (p-value = 0.01; $\log(\mathbb{E}(B|L, W)) = -4.02 +$
528 $0.50W + 0.12L$, where $W = 1$ for WT). For (O) the best-fitting relationship indicated WT was
529 smaller than *tarac* at all lengths (p-value=0.006; $\log(\mathbb{E}(B|L, W)) = -1.94 - 0.73W + 0.095L$,
530 where $W = 1$ for WT). **(P)** The position of the lowermost branch was closer to the
531 gametophore base in *tarac* than in *tara* or *tarc* in comparison with WT (Wilcoxon rank sum
532 test with continuity correction different from WT, *p-value ≤ 0.05 ; WT versus *tara*, p-value =
533 0.30 ; WT versus *tarc*, p-value = 0.12 ; WT versus *tarac*, p-value = 0.007).
534



535

536 **Figure 4. *YUCC* and *YUCF* genes repress branching. (A-D)** Branching patterns in WT, *yucc*,

537 *yucf* and *yuccf* mutants. Brackets indicate the three lowermost metamers. (E-H) WT (E), *yucc*

538 (F), *yucf* (G) and *yuccf* (H) gametophores before (left) and after (right) removing leaves, with

539 asterisks marking branches. Scale bars represent 1 mm. (I) There was strong and moderate

540 evidence that the apical inhibition zone was different in *yucc* and *yuccf* mutants, respectively,

541 compared with wild-type control (Wilcoxon rank sum test with continuity correction different

542 from WT, * p -value ≤ 0.05 ; WT versus *yucc*, p -value = 0.003 ; WT versus *yucf*, p -value = 0.82 ;

543 WT versus *tarac*, p -value = 0.05). (J) There was strong evidence that the distance to the

544 closest branch, a measurement of branch spacing, was reduced in *yuccf* double mutants,

545 but not in *yucc* or *yucf* single mutants, compared with wild-type control (Wilcoxon rank sum

546 test with continuity correction different from WT, * p -value ≤ 0.05 ; WT versus *yuc*, p -value =

547 0.77 ; WT versus *yucf*, p -value = 0.76 ; WT versus *yuccf*, p -value = 0.01). (K) There was very

548 strong evidence that the position of the lowermost branch was closer to the gametophore

549 base in *yuccf* than in *yucc* or *yucf* in comparison with WT (Wilcoxon rank sum test with

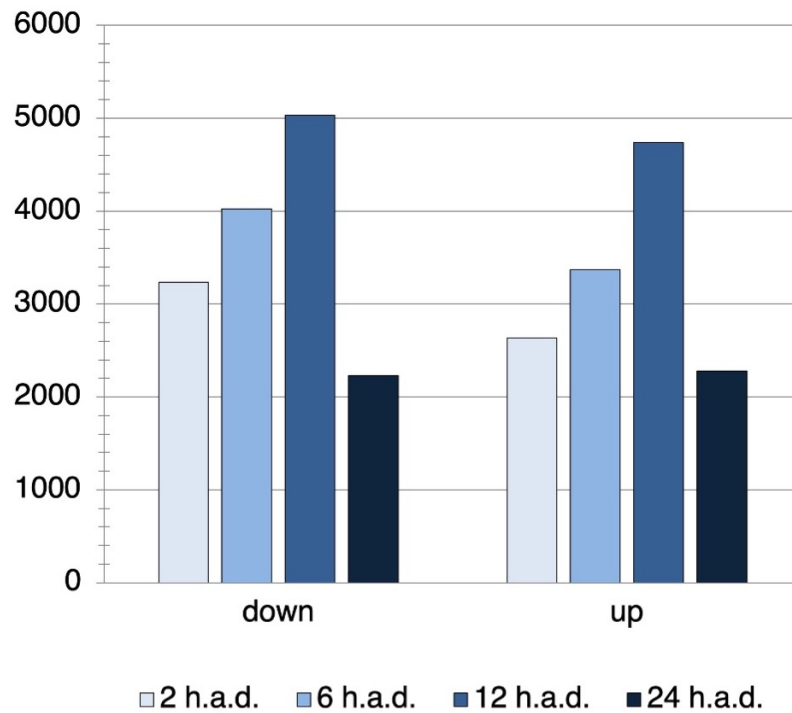
550 continuity correction different from WT, * p -value ≤ 0.05 ; WT versus *yucc*, p -value = 0.49 ;

551 WT versus *yucf*, p-value = 0.34 ; WT versus *yuccf*, p-value = 0.0006). **(L-M)** Bubble plots
552 showed that branch number responded differently to length in all three mutants compared
553 with WT. Gametophore length is represented as the number of metamers and the bubble
554 area is proportional to the number of gametophores with the same branch number (B) at a
555 given length (L). The data were not over-dispersed, and so Poisson regression was used to
556 test whether and how the relationship between branch number and gametophore length
557 depended on treatment (see ‘Material and methods’). The best-fitting relationship included
558 an interaction for all three mutants, indicating the nature of the difference in the number of
559 branches between WT and mutant depended upon the length (in (L), $p = 0.002$,
560 $\log(\mathbb{E}(B|L, Y)) = -5.28 + 3.17Y + (0.20 - 0.10Y)L$, where $Y = 1$ for *yucc*; in (M) $p = 0.03$,
561 $\log(\mathbb{E}(B|L, Y)) = -5.28 + 2.25Y + (0.20 - 0.07Y)L$, where $Y = 1$ for *yucf*; in (N) $p = 0.02$,
562 $\log(\mathbb{E}(B|L, Y)) = -5.28 + 3.25Y + (0.20 - 0.08Y)L$, where $Y = 1$ for *yuccf*).

563 **Supplementary data**

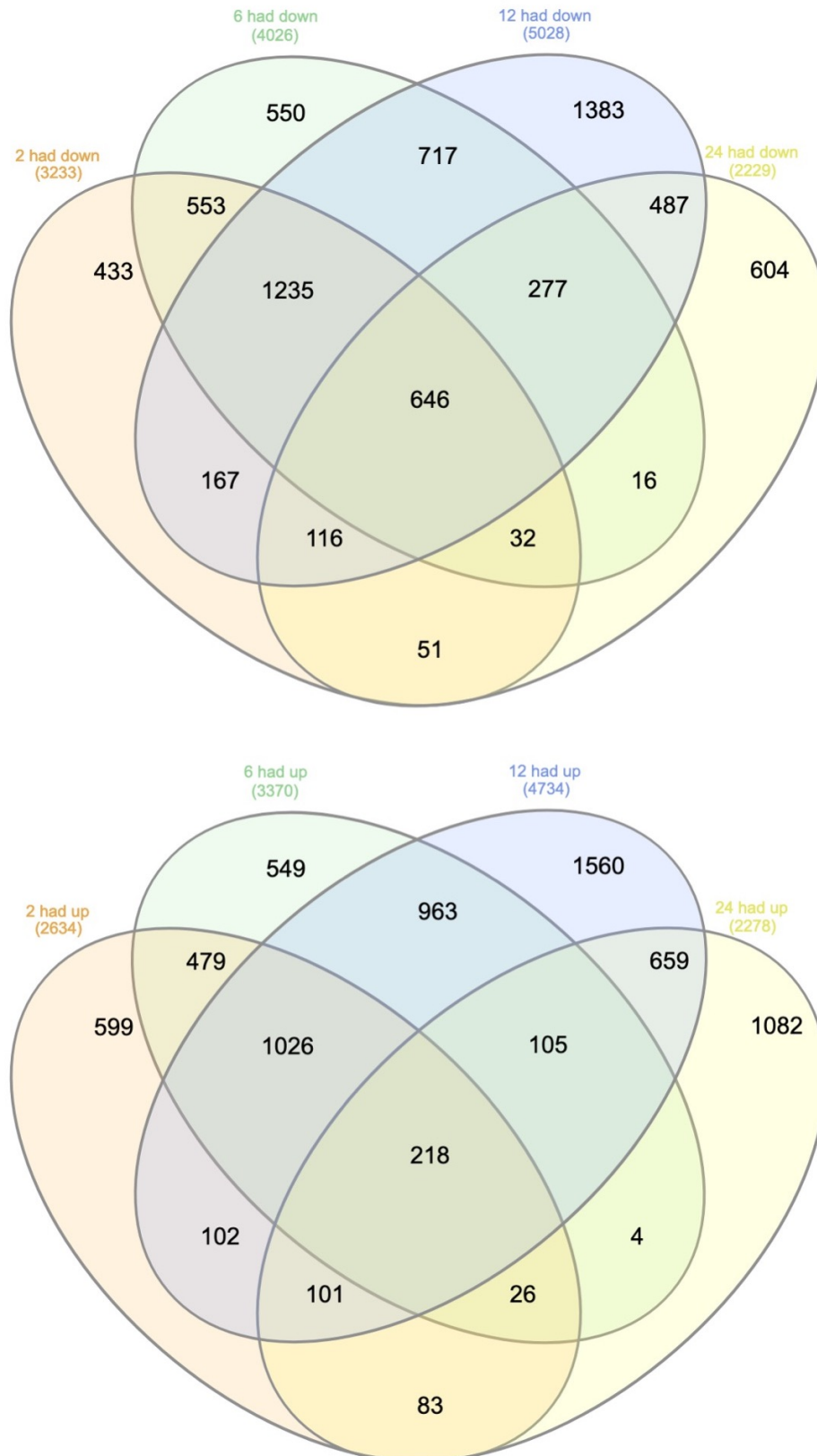
564

565



566

567 **Figure S1. Number of genes repressed or induced 2, 6, 12 and 24 hours after**
568 **decapitation.**



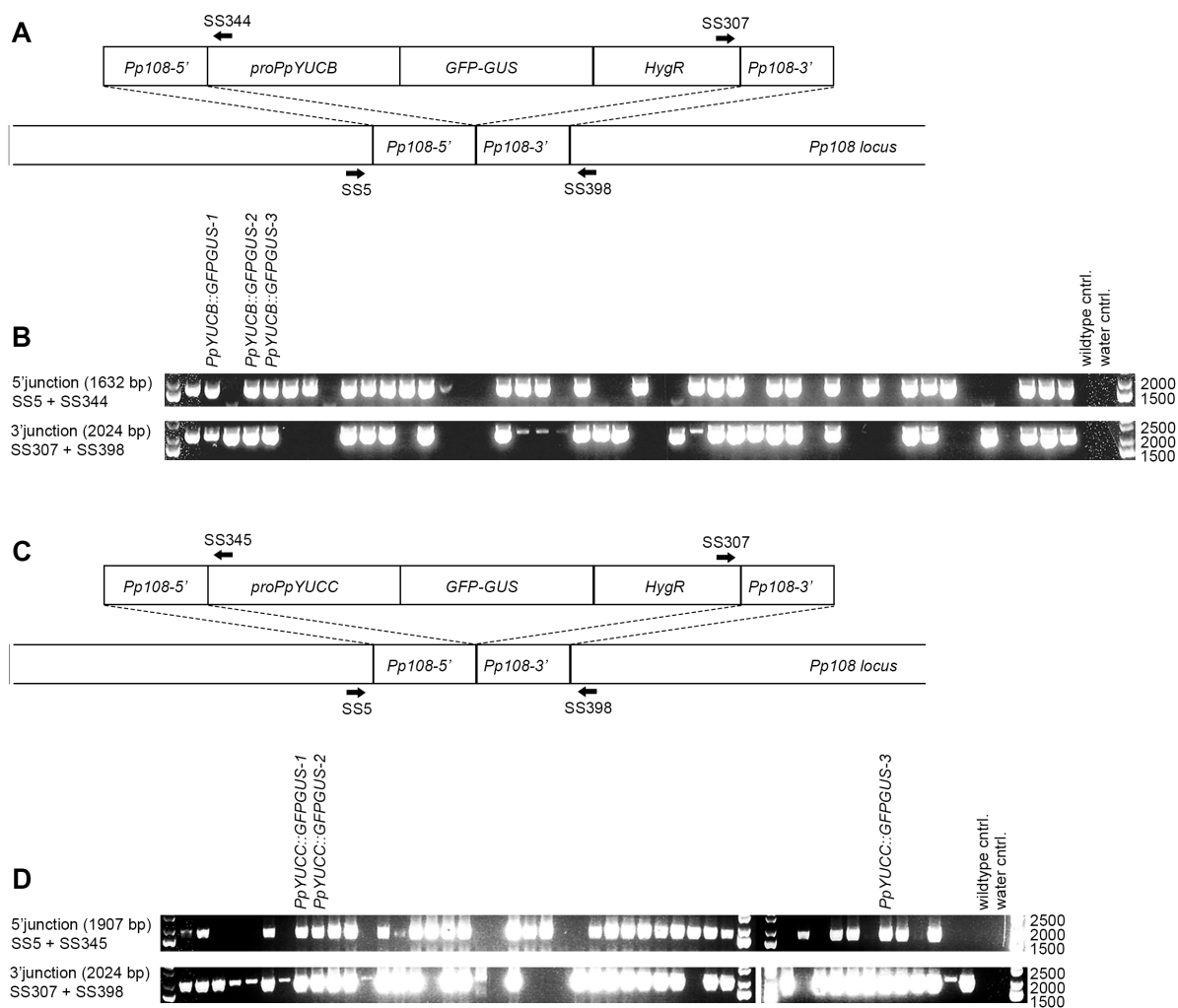
569

570

571 **Figure S2. Venn diagrams for all genes repressed or induced 2, 6, 12 and 24 hours after**

572 **decapitation.**

573



574

575

576 **Figure S3. PCR verification of *PpYUCB* and *PpYUCC* transcriptional reporter lines in**

577 **WT background (A)** Schematic view of the *PpYUCB*::*GFPUS* reporter construct pMT244

578 and the *Pp108* locus to which it was targeted. Arrows mark the approximate annealing sites

579 of primers used for PCR verification in B. **(B)** PCR verification of 5' and 3' junctions to confirm

580 correct integration of the *PpYUCB*::*GFPUS* reporter construct into the *Pp108* locus. **(C)**

581 Schematic view of the *PpYUCC*::*GFPUS* reporter construct pMT251 and the *Pp108* locus

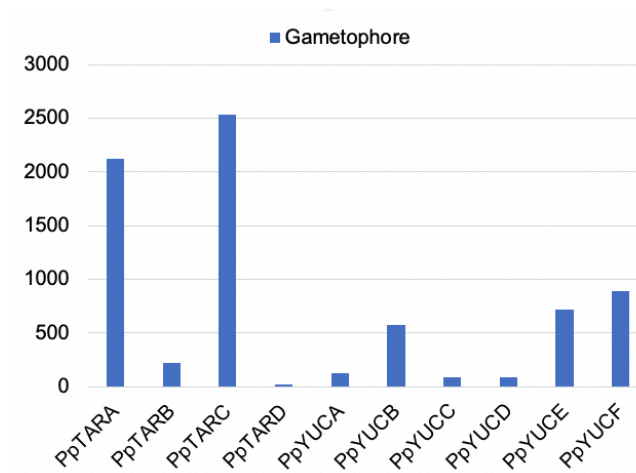
582 to which it was targeted. Arrows mark the approximate annealing sites of primers used for

583 PCR verification in D. **(D)** PCR verification of 5' and 3' junctions to confirm correct integration

584 of the *PpYUCC*::*GFPUS* reporter construct into the *Pp108* locus. In both B and D, expected

585 product sizes are indicated within parentheses. For primer sequences, see Table S5.

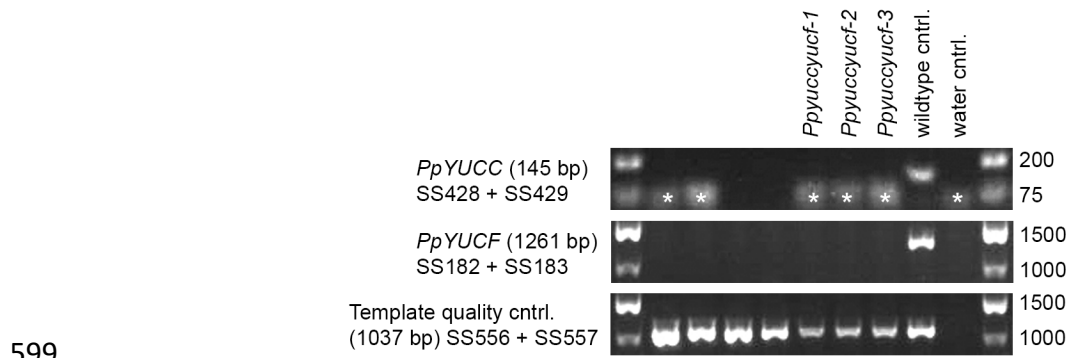
586



587
588

589 **Figure S4. Absolute expression levels of *TAR* and *YUC* genes in *Physcomitrium patens***
590 **gametophores retrieved from Ortiz-Ramirez *et al.* (2016)⁵⁰.** Correspondence between
591 gene names and identifiers: *PpTARA* (Pp3c21_15370V3.1, Pp1s167_103V6.1), *PpTARB*
592 (Pp3c18_15140V3.1, Pp1s3_273V6.1), *PpTARC* (Pp3c17_6500V3.1, Pp1s26_28V6.1),
593 *PpTARD* (Pp3c26_12520V3.1, Pp1s6_329V6.1), *PpYUCA* (Pp3c3_18590V1.1,
594 Pp1s312_60V6.1), *PpYUCB* (Pp3c11_11790V3.1, Pp1s11_6V6.1), *PpYUCC*
595 (Pp3c1_11500V3.1, Pp1s139_131V6.1), *PpYUCD* (Pp3c2_27740V3.1, Pp1s22_291V6.1),
596 *PpYUCE* (Pp3c13_21970V3.1, Pp1s37_90V6.1), *PpYUCF* (Pp3c3_20490V3.1,
597 Pp1s204_126V6.1).

598



599

600

601 **Figure S5. PCR genotyping of *yuccf* double knockout lines produced by a sexual cross**

602 **of the single knockout lines *Ppyucc-2* and *Ppyucf-1* (Landberg et al., 2020)¹⁸.** The upper

603 panel shows the result for a PCR confirming the loss of an internal *PpYUCC* gene sequence.

604 Asterisks mark primer dimers. The middle panel shows the result for a PCR confirming the

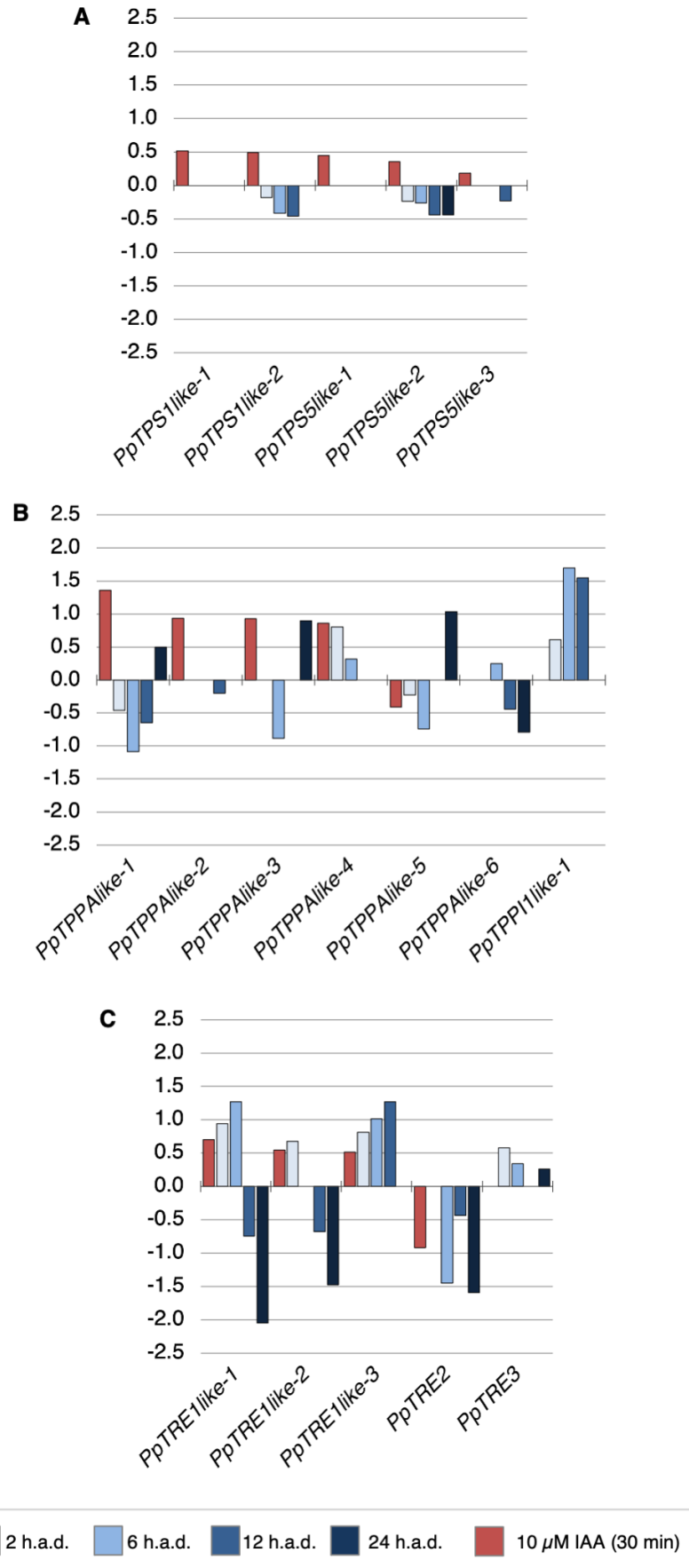
605 loss of an internal *PpYUCF* gene sequence. The bottom panel shows amplification of an

606 unrelated locus to confirm integrity of the gDNA used as template in all three panels. Next to

607 each panel, the primers used and the expected product size are noted. For primer sequences,

608 see Table S5.

609



611 **Figure S6. Expression of trehalose-6-phosphate (T6P) metabolism genes is affected by**
612 **exogenous auxin and gametophore decapitation.** Bar plots show \log_2 fold-change in
613 expression of *T6P synthase* (*PpTPS*), *T6P phosphatase* (*PpTPP*) and *trehalase* (*PpTRE*)
614 coding genes in wild-type *Physcomitrium patens* gametophores after treatment with auxin
615 (red bars) or decapitation (blue bars). Correspondence between gene names and identifiers:
616 *PpTPPAlike-1* (Pp3c12_20050V3.1), *PpTPPAlike-2* (Pp3c4_20080V3.1), *PpTPPAlike-3*
617 (Pp3c4_11080V3.1), *PpTPPAlike-4* (Pp3c10_13170V3.1), *PpTPPAlike-5* (Pp3c3_25080V3.1),
618 *PpTPPAlike-6* (Pp3c3_22990V3.1), *PpTPPC1like-1* (Pp3c12_7510V3.1), *PpTPPE1like-1*
619 (Pp3c12_7530V3.1), *PpTPPI1like-1* (Pp3c10_23130V3.1), *PpTPS1like-1* (Pp3c5_17730V3.1),
620 *PpTPS1like-2* (Pp3c6_16450V3.1), *PpTPS5like-1* (Pp3c25_6990V3.1), *PpTPS5like-2*
621 (Pp3c11_17560V3.1), *PpTPS5like-3* (Pp3c7_15250V3.1), *PpTRE1like-1* (Pp3c5_16470V3.1),
622 *PpTRE1like-2* (Pp3c23_11240V3.1), *PpTRE1like-3* (Pp3c16_7830V3.1), *PpTRE1like-4*
623 (Pp3c24_9748V3.1), *PpTRE1like-5* (Pp3c24_9750V3.1), *PpTRE2* (Pp3c6_4940V3.1), *PpTRE3*
624 (Pp3c10_5310V3.1).

625

626

627 **Acknowledgements**

628 YC acknowledges Fabrice Besnard, Joe Cammarata and Teva Vernoux for constructive
629 discussions and suggestions on a draft version of this article, Stéphanie Hallet for technical
630 support, and the CNRS (ATIP-Avenir programme) for research funding. The sequencing
631 platform (POPS) benefited from the support of the LabEx Saclay Plant Sciences-SPS (ANR-
632 10-LABX-0040-SPS).

633

634

635 **References**

- 636 1. Coudert, Y., Bell, N.E., Edelin, C., and Harrison, C.J. (2017). Multiple innovations
637 underpinned branching form diversification in mosses. *New Phytol* 22, 810.
- 638 2. Coudert, Y., Palubicki, W., Ljung, K., Novak, O., Leyser, O., and Harrison, C.J. (2015).
639 Three ancient hormonal cues co-ordinate shoot branching in a moss. *eLife* 4, e06808.
- 640 3. Domagalska, M.A., and Leyser, O. (2011). Signal integration in the control of shoot
641 branching. *Nat Rev Mol Cell Biol* 12, 211–221.
- 642 4. Ferguson, B.J., and Beveridge, C.A. (2009). Roles for auxin, cytokinin, and strigolactone
643 in regulating shoot branching. *Plant Physiol* 149, 1929–1944.
- 644 5. Coudert, Y., Harris, S., and Charrier, B. (2019). Design Principles of Branching
645 Morphogenesis in Filamentous Organisms. *Curr. Biol.* 29, R1149–R1162.

- 646 6. Barthélémy, D., and Caraglio, Y. (2007). Plant architecture: a dynamic, multilevel and
647 comprehensive approach to plant form, structure and ontogeny. *Ann Bot* 99, 375–407.
- 648 7. Coudert, Y. (2017). The Evolution of Branching in Land Plants: Between Conservation
649 and Diversity. In *Evolutionary Developmental Biology* (Springer International Publishing),
650 pp. 1–17.
- 651 8. Cline, M. (1997). Concepts and terminology of apical dominance. *Am J Bot* 84, 1064.
- 652 9. Von Maltzahn, K. (1959). Interaction between Kinetin and Indoleacetic Acid in the Control
653 of Bud Reactivation in *Splachnum ampullaceum* (L.) Hedw. *Nature* 183, 60–61.
- 654 10. Eklund, D.M., Thelander, M., Landberg, K., Ståldal, V., Nilsson, A., Johansson, M.,
655 Valsecchi, I., Pederson, E.R.A., Kowalczyk, M., Ljung, K., et al. (2010). Homologues of
656 the *Arabidopsis thaliana* SHI/STY/LRP1 genes control auxin biosynthesis and affect
657 growth and development in the moss *Physcomitrella patens*. *Development* 137, 1275–
658 1284.
- 659 11. Sohlberg, J.J., Myrenås, M., Kuusk, S., Lagercrantz, U., Kowalczyk, M., Sandberg,
660 G., and Sundberg, E. (2006). STY1 regulates auxin homeostasis and affects apical–basal
661 patterning of the *Arabidopsis* gynoecium. *The Plant Journal* 47, 112–123.
- 662 12. Lavy, M., Prigge, M.J., Tao, S., Shain, S., Kuo, A., Kirchsteiger, K., Estelle, M., and
663 Hardtke, C.S. (2016). Constitutive auxin response in *Physcomitrella* reveals complex
664 interactions between Aux/IAA and ARF proteins. *eLife Sciences* 5, e13325.
- 665 13. Thelander, M., Landberg, K., and Sundberg, E. (2018). Auxin-mediated
666 developmental control in the moss *Physcomitrella patens*. *J Exp Bot* 69, 277–290.
- 667 14. Yadav, S., Kumar, H., and Yadav, R.K. (2020). Local auxin biosynthesis promotes
668 shoot patterning and stem cell differentiation in *Arabidopsis* shoot apex. *bioRxiv*,
669 819342.
- 670 15. Galvan-Ampudia, C.S., Cerutti, G., Legrand, J., Brunoud, G., Martin-Arevalillo, R.,
671 Azais, R., Bayle, V., Moussu, S., Wenzl, C., Jaillais, Y., et al. (2020). Temporal integration
672 of auxin information for the regulation of patterning. *eLife* 9, e55832.
- 673 16. Cheng, Y., Dai, X., and Zhao, Y. (2006). Auxin biosynthesis by the YUCCA flavin
674 monooxygenases controls the formation of floral organs and vascular tissues in
675 *Arabidopsis*. *Genes Dev.* 20, 1790–1799.
- 676 17. Ljung, K. (2013). Auxin metabolism and homeostasis during plant development.
677 *Development* 140, 943–950.
- 678 18. Landberg, K., Šimura, J., Ljung, K., Sundberg, E., and Thelander, M. (2021). Studies
679 of moss reproductive development indicate that auxin biosynthesis in apical stem cells
680 may constitute an ancestral function for focal growth control. *New Phytologist* 229, 845–
681 860.
- 682 19. Kawai, Y., Ono, E., and Mizutani, M. (2014). Evolution and diversity of the 2-
683 oxoglutarate-dependent dioxygenase superfamily in plants. *Plant J* 78, 328–343.
- 684 20. Muff, S., Nilsen, E.B., O’Hara, R.B., and Nater, C.R. (2021). Rewriting results
685 sections in the language of evidence. *Trends in Ecology & Evolution* 0.

- 686 21. Bennett, T.A., Liu, M.M., Aoyama, T., Bierfreund, N.M., Braun, M., Coudert, Y.,
687 Dennis, R.J., O'Connor, D., Wang, X.Y., White, C.D., et al. (2014). Plasma Membrane-
688 Targeted PIN Proteins Drive Shoot Development in a Moss. *Curr. Biol.* *24*, 2776–2785.
- 689 22. Lang, D., Ullrich, K.K., Murat, F., Fuchs, J., Jenkins, J., Haas, F.B., Piednoel, M.,
690 Gundlach, H., Van Bel, M., Meyberg, R., et al. (2018). The *Physcomitrella patens*
691 chromosome-scale assembly reveals moss genome structure and evolution. *The Plant*
692 *Journal* *93*, 515–533.
- 693 23. Romani, F. (2017). Origin of TAA Genes in Charophytes: New Insights into the
694 Controversy over the Origin of Auxin Biosynthesis. *Front. Plant Sci.* *8*, R899-3.
- 695 24. Delaux, P.-M., Hetherington, A.J., Coudert, Y., Delwiche, C., Dunand, C., Gould, S.,
696 Kenrick, P., Li, F.-W., Philippe, H., Rensing, S.A., et al. (2019). Reconstructing trait
697 evolution in plant evo-devo studies. *Curr. Biol.* *29*, R1110–R1118.
- 698 25. Eklund, D.M., Ishizaki, K., Flores-Sandoval, E., Kikuchi, S., Takebayashi, Y.,
699 Tsukamoto, S., Hirakawa, Y., Nonomura, M., Kato, H., Kouno, M., et al. (2015). Auxin
700 Produced by the Indole-3-Pyruvic Acid Pathway Regulates Development and Gemmae
701 Dormancy in the Liverwort *Marchantia polymorpha*. *The Plant Cell Online* *27*, 1650–1669.
- 702 26. Solly, J.E., Cunniffe, N.J., and Harrison, C.J. (2017). Regional Growth Rate
703 Differences Specified by Apical Notch Activities Regulate Liverwort Thallus Shape.
704 *Current Biology* *27*, 16–26.
- 705 27. Shubin, N., Tabin, C., and Carroll, S. (2009). Deep homology and the origins of
706 evolutionary novelty. *Nature* *457*, 818–823.
- 707 28. Véron, E., Vernoux, T., and Coudert, Y. (2020). Phyllotaxis from a Single Apical Cell.
708 *Trends in Plant Science*.
- 709 29. Toyokura, K., Goh, T., Shinohara, H., Shinoda, A., Kondo, Y., Okamoto, Y., Uehara,
710 T., Fujimoto, K., Okushima, Y., Ikeyama, Y., et al. (2019). Lateral Inhibition by a Peptide
711 Hormone-Receptor Cascade during Arabidopsis Lateral Root Founder Cell Formation.
712 *Dev Cell* *48*, 64-75.e5.
- 713 30. Chandler, J.W., and Werr, W. (2017). DORNROESCHEN, DORNROESCHEN-LIKE, and
714 PUCHI redundantly control floral meristem identity and organ initiation in Arabidopsis. *J*
715 *Exp Bot* *68*, 3457–3472.
- 716 31. Capua, Y., and Eshed, Y. (2017). Coordination of auxin-triggered leaf initiation by
717 tomato LEAFLESS. *Proc Natl Acad Sci USA* *114*, 3246–3251.
- 718 32. Ishikawa, M., Morishita, M., Higuchi, Y., Ichikawa, S., Ishikawa, T., Nishiyama, T.,
719 Kabeya, Y., Hiwatashi, Y., Kurata, T., Kubo, M., et al. (2019). *Physcomitrella* STEMIN
720 transcription factor induces stem cell formation with epigenetic reprogramming. *Nat*
721 *Plants* *5*, 681–690.
- 722 33. Fichtner, F., Barbier, F.F., Feil, R., Watanabe, M., Annunziata, M.G., Chabikwa, T.G.,
723 Höfgen, R., Stitt, M., Beveridge, C.A., and Lunn, J.E. (2017). Trehalose 6-phosphate is
724 involved in triggering axillary bud outgrowth in garden pea (*Pisum sativum* L.). *The Plant*
725 *Journal* *92*, 611–623.

- 726 34. Fichtner, F., Barbier, F.F., Annunziata, M.G., Feil, R., Olas, J.J., Mueller-Roeber, B.,
727 Stitt, M., Beveridge, C.A., and Lunn, J.E. (2021). Regulation of shoot branching in
728 arabidopsis by trehalose 6-phosphate. *New Phytol* 229, 2135–2151.
- 729 35. Satoh-Nagasawa, N., Nagasawa, N., Malcomber, S., Sakai, H., and Jackson, D.
730 (2006). A trehalose metabolic enzyme controls inflorescence architecture in maize.
731 *Nature* 441, 227–230.
- 732 36. Claeys, H., Vi, S.L., Xu, X., Satoh-Nagasawa, N., Eveland, A.L., Goldshmidt, A., Feil,
733 R., Beggs, G.A., Sakai, H., Brennan, R.G., et al. (2019). Control of meristem determinacy
734 by trehalose 6-phosphate phosphatases is uncoupled from enzymatic activity. *Nature*
735 *Plants*, 1–9.
- 736 37. Hiss, M., Meyberg, R., Westermann, J., Haas, F.B., Schneider, L., Schallenberg-
737 Rüdinger, M., Ullrich, K.K., and Rensing, S.A. (2017). Sexual reproduction, sporophyte
738 development and molecular variation in the model moss *Physcomitrella patens*:
739 introducing the ecotype Reute. *The Plant Journal* 22, 9.
- 740 38. Thelander, M., Landberg, K., and Sundberg, E. (2019). Minimal auxin sensing levels
741 in vegetative moss stem cells revealed by a ratiometric reporter. *New Phytologist* 224,
742 775–788.
- 743 39. Schaefer, D., Zryd, J.P., Knight, C.D., and Cove, D.J. (1991). Stable transformation
744 of the moss *Physcomitrella patens*. *Mol Gen Genet* 226, 418–424.
- 745 40. Rensing, S.A., Lang, D., Zimmer, A.D., Terry, A., Salamov, A., Shapiro, H.,
746 Nishiyama, T., Perroud, P.-F., Lindquist, E.A., Kamisugi, Y., et al. (2008). The
747 *Physcomitrella* genome reveals evolutionary insights into the conquest of land by plants.
748 *Science* 319, 64–69.
- 749 41. Gagnot, S., Tamby, J.-P., Martin-Magniette, M.-L., Bitton, F., Taconnat, L.,
750 Balzergue, S., Aubourg, S., Renou, J.-P., Lecharny, A., and Brunaud, V. (2008). CATdb: a
751 public access to Arabidopsis transcriptome data from the URGV-CATMA platform.
752 *Nucleic Acids Research* 36, D986–D990.
- 753 42. Kopylova, E., Noé, L., and Touzet, H. (2012). SortMeRNA: fast and accurate filtering
754 of ribosomal RNAs in metatranscriptomic data. *Bioinformatics* 28, 3211–3217.
- 755 43. Langmead, B., and Salzberg, S.L. (2012). Fast gapped-read alignment with Bowtie
756 2. *Nat Methods* 9, 357–359.
- 757 44. Rigaille, G., Balzergue, S., Brunaud, V., Blondet, E., Rau, A., Rogier, O., Caius, J.,
758 Maugis-Rabusseau, C., Soubigou-Taconnat, L., Aubourg, S., et al. (2018). Synthetic data
759 sets for the identification of key ingredients for RNA-seq differential analysis. *Briefings in*
760 *Bioinformatics* 19, 65–76.
- 761 45. McCarthy, D.J., Chen, Y., and Smyth, G.K. (2012). Differential expression analysis of
762 multifactor RNA-Seq experiments with respect to biological variation. *Nucleic Acids*
763 *Research* 40, 4288–4297.
- 764 46. Heberle, H., Meirelles, G.V., da Silva, F.R., Telles, G.P., and Minghim, R. (2015).
765 InteractiVenn: a web-based tool for the analysis of sets through Venn diagrams. *BMC*
766 *Bioinformatics* 16, 169.

- 767 47. Ge, S.X., Jung, D., and Yao, R. (2020). ShinyGO: a graphical gene-set enrichment
768 tool for animals and plants. *Bioinformatics* 36, 2628–2629.
- 769 48. Edgar, R., Domrachev, M., and Lash, A.E. (2002). Gene Expression Omnibus: NCBI
770 gene expression and hybridization array data repository. *Nucleic Acids Research* 30,
771 207–210.
- 772 49. Kleiber, C., and Zeileis, A. (2020). *AER: Applied Econometrics with R*.
- 773 50. Ortiz-Ramírez, C., Hernandez-Coronado, M., Thamm, A., Catarino, B., Wang, M.,
774 Dolan, L., Feijó, J.A., and Becker, J.D. (2016). A Transcriptome Atlas of *Physcomitrella*
775 *patens* Provides Insights into the Evolution and Development of Land Plants. *Mol Plant*
776 9, 205–220.
- 777